



Title	Application of a simple DNA damage model developed for electrons to proton irradiation
Author(s)	Matsuya, Yusuke; Kai, Takeshi; Parisi, Alessio; Yoshii, Yuji; Sato, Tatsuhiko
Citation	Physics in medicine and biology, 67(21), 215017 https://doi.org/10.1088/1361-6560/ac9a20
Issue Date	2022-10-31
Doc URL	http://hdl.handle.net/2115/90631
Rights	This is the Accepted Manuscript version of an article accepted for publication in Physics in Medicine & Biology. IOP Publishing Ltd is not responsible for any errors or omissions in this version of the manuscript or any version derived from it. The Version of Record is available online at https://doi.org/10.1088/1361-6560/ac9a20 .
Rights(URL)	https://creativecommons.org/licenses/by-nc-nd/4.0/
Type	article (author version)
File Information	Matsuya2022.pdf



[Instructions for use](#)

Application of a simple DNA damage model developed for electrons to proton irradiation

Yusuke Matsuya^{1*}, Takeshi Kai¹, Alessio Parisi^{2,3}, Yuji Yoshii⁴ and Tatsuhiko Sato¹

¹ Nuclear Science and Engineering Center, Japan Atomic Energy Agency, Tokai, Ibaraki, Japan

² Radiation Protection Dosimetry and Calibration Expert Group, Belgian Nuclear Research Centre, Mol, Belgium

³ Department of Radiation Oncology, Mayo Clinic, Jacksonville, Florida, USA

⁴ Central Institute of Isotope Science, Hokkaido University, Sapporo, Hokkaido, Japan

*Corresponding author: matsuya.yusuke@jaea.go.jp (Yusuke Matsuya)

ABSTRACT

Proton beam therapy allows irradiating tumor volumes with reduced side effects on normal tissues with respect to conventional X-ray radiotherapy. Biological effects such as cell killing after proton beam irradiations depend on the proton kinetic energy, which is intrinsically related to early DNA damage induction. As such, DNA damage estimation based on Monte Carlo simulations is a research topic of worldwide interest. Such simulation is a mean of investigating the mechanisms of DNA strand break formations. However, past modellings considering chemical processes and DNA structures require long calculation times. Particle and Heavy Ion Transport System (PHITS) is one of the general-purpose Monte Carlo codes that can simulate track structure of protons, meanwhile cannot handle radical dynamics simulation in liquid water. It also includes a simple model enabling the efficient estimation of DNA damage yields only from the spatial distribution of ionizations and excitations without DNA geometry, which was originally developed for electron track-structure simulations. In this study, we investigated the potential application of the model to protons without any modification. The yields of single-strand breaks, double-strand breaks (DSBs) and the complex DSBs were assessed as functions of the proton kinetic energy. The PHITS-based estimation showed that the DSB yields increased as the linear energy transfer (LET) increased, and reproduced the experimental and simulated yields of various DNA damage types induced by protons with LET up to about 30 keV/μm. These results suggest that the current DNA damage model implemented in PHITS is sufficient for estimating DNA lesion yields induced after protons irradiation except at very low energies (below 1 MeV). This model contributes to evaluating early biological impacts in radiation therapy.

Keywords: DNA damage yields, Monte Carlo track-structure simulation, proton beams,

1. INTRODUCTION

Proton beam therapy (PBT), which has been widely installed in clinics, is one of the effective approaches to eliminate solid tumors by dose concentrations to a tumor at the Bragg

41 peak region (1,2). The biological impacts for PBT relative to photon beams (referred to as
42 relative biological effectiveness [RBE]) is generally defined as 1.1 (2) because of the major
43 contribution of secondary electrons (3) interacting with DNA (liquid water). However, it has
44 been proposed that the use of a constant RBE = 1.1 for protons is no longer appropriate (4,5).
45 Therefore, quantifying the variable RBE value depending on proton energy (i.e., the increase
46 in RBE at the Bragg peak region) from the standpoints of radiation therapy and radiation
47 biology is necessary.

48 When quantifying such RBE value of PBT, tumor cell killing is usually evaluated.
49 Several reports show that cell death (such as apoptosis, necrosis, and autophagy (6)) is induced
50 by radiation-induced DNA double-strand breaks (DSBs) with a certain probability (7-10). As
51 such, the dependence of proton energy (as well as linear energy transfer [LET]) on DSB
52 induction has been evaluated to date (11). There are several techniques for measuring DSB
53 yields (e.g., immunofluorescent staining and agarose gel electrophoresis). (12-15). The DSB
54 yields for any proton energies can be quantified using both plasmid DNA and cultured cell lines
55 based on such experimental techniques. However, the yields for low-energy protons (i.e., < 1
56 MeV protons) can be obtained only by dry plasmid DNA (16) as low-energy protons have a
57 correspondingly short range in water. For example, the ranges of 1 MeV and 300 keV protons
58 are approximately 23.9 and 3.78 μm , respectively. When performing such experiments *in vitro*,
59 the yields can vary depending on the experimental conditions, that is, cell shape (17) and
60 plasmid condition (liquid or dry) (18). Therefore, grasping experimental geometry and the
61 proton kinetics in the biomaterials is necessary for obtaining the relationship between proton
62 energy and DNA damage yields.

63 Monte Carlo simulations are an efficient approach to mechanistically investigate the
64 relationship between proton energy (as well as LET) and DNA damage yields. In particular,
65 track-structure simulation at the DNA level (nanometer scale) in liquid water (19-21) enables
66 mechanistically estimating DNA damage yields and types (i.e., single-strand breaks [SSBs],
67 DSBs, and complex DSBs) (22-25) even for low-energy protons (i.e., < 1 MeV protons). The
68 past modellings for estimating DNA damage yields have considered chemical processes (free
69 radicals) and DNA structures in detail (26,27). However, the past modellings which consider
70 chemical processes and DNA structure need a long calculation time. Recently, DNA damage
71 estimation is getting more and more attention in the field of medical physics (28,29). In order
72 to reduce computing time, simplified models of evaluating DNA damage induction are of
73 interest. However, at the price of computing time reduction, these simplified models can only
74 simulate the physical stage of radiation interaction and do not model radical diffusion nor
75 chemical reactions. With reasonable short computing time, estimating DNA damage yields with
76 high precision is therefore of great importance as mechanism study.

77 Several similar approaches, such as density-based spatial clustering of applications with
78 noise (DBSCAN) (30) and ion cluster size distribution (31) have been proposed. However, by
79 focusing on only the number and the distance of the events (ionizations and excitations), we

80 developed a simple model for efficiently estimating DNA damage yields (32-34) by the track-
81 structure mode in the Particle and Heavy Ion Transport System (PHITS) (35-37). This model
82 enables efficiently estimating DNA damage types and yields only using spatial distribution of
83 ionizations and excitations where track-structure mode is activated. In addition, in the recent
84 PHITS development, the physical models of Kyushu University Radiobiology Unit Code
85 (KURBUC) of protons and Carbon ions was implemented in PHITS under the name of *PHITS-*
86 *KURBUC* mode, which enables simulating atomic interactions (i.e., elastic scattering,
87 ionization, excitation, dissociative electron attachment, vibrational excitation, photon excitation,
88 rotational excitation, electron capture, and electron loss) of protons in liquid water (36).
89 Meanwhile, the current PHITS code does not explicitly simulate radical diffusion and chemical
90 reactions to DNA. To date, the DNA damage model in PHITS has been verified only for
91 electron (as well as photon) irradiation (32-34). The estimation of DNA damage yields for
92 proton irradiation is in principle possible with the PHITS code but has not been investigated
93 yet.

94 In this study, applying the simplified model to proton irradiation, we evaluated the yields
95 of SSBs, DSBs, and complex DSBs for proton beams, and compared them with the
96 corresponding experimental data and other simulation results. From the comprehensive
97 comparisons, we discussed the effectiveness of the current DNA damage estimation model
98 based on the PHITS track-structure simulation mode in the case of proton beam irradiations.
99 Throughout this evaluation, we show the simple DNA damage estimation model implemented
100 in the PHITS code would contribute to understanding early biological impacts in PBT.

101

102 **2. MATERIALS AND METHODS**

103 *2-1. Simulation setup and physical processes*

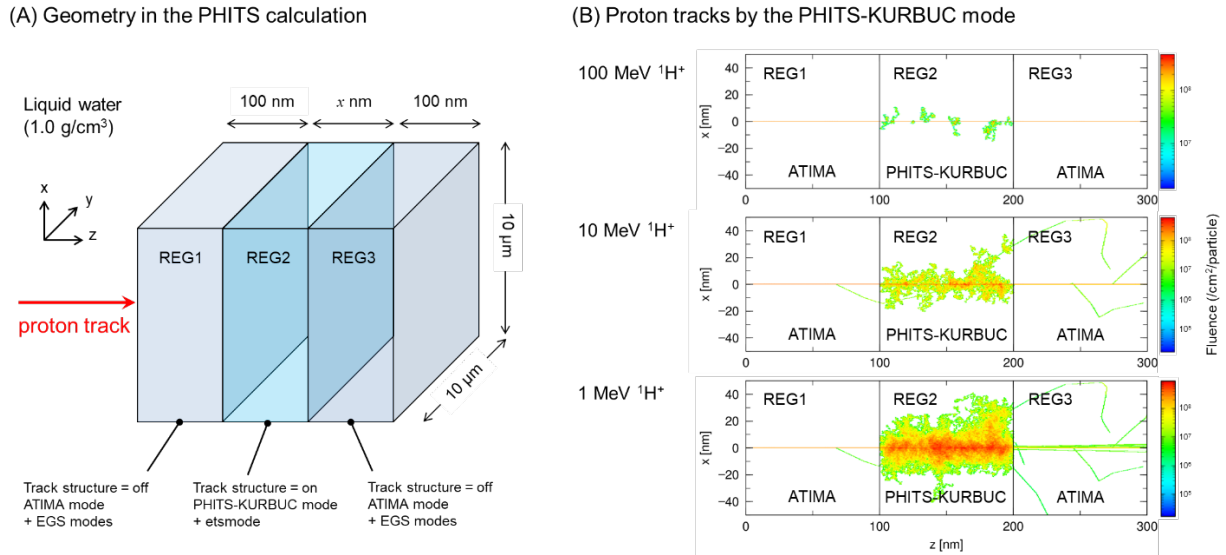
104 We used PHITS ver. 3.27 (35) and simulated electron and proton tracks using two model
105 types: one is the condensed-history method for the macroscopic scale and the other is the track-
106 structure mode for the microscopic scale (DNA scale). For the condensed-history method, the
107 ATIMA mode (38) and the electron gamma shower (EGS) mode (39) were used, and the
108 transport cut-off energies were set to 1 keV for both electrons and protons. For the track-
109 structure simulations, the electron track-structure mode (*etsmode*) (32) and the proton track-
110 structure *PHITS-KURBUC* mode (36) were used to simulate atomic interactions along proton
111 track in the region where the track-structure section is activated. In the track-structure
112 simulations, the cut-off energies for transporting electrons and protons were 1 eV and 1 keV,
113 respectively.

114

115 *2-2. Estimation of SSB and DSB yields*

116 The simple geometry composed of three cuboids illustrated in Fig. 1A was considered for
117 estimating proton-induced DNA damage yields. In this geometry, the track-structure mode was
118 activated in the central region (REG2), while the condensed history approach was taken in

119 REG1 and REG3. Examples of simulated proton tracks are depicted in Fig. 1B, where 10 tracks
 120 of 100, 10 and 1 MeV protons were simulated. The thickness of REG2 was defined to be large
 121 enough that at least 1% of the proton energy is being deposited in this region. For example, for
 122 1 MeV protons a thickness of 382 nm is needed. For higher energies, larger thicknesses would
 123 be needed, however, this would result in long computing times. Hence, for proton energies
 124 larger than 1 MeV, a constant thickness of 1 μm was chosen. Meanwhile, judged from radial
 125 dose distribution, secondary electrons deposit their energy and almost stop within 100 nm from
 126 proton track (34). Considering this, 100 nm was chosen as the thicknesses of REG1 and REG3.
 127 Using this geometry, we simulated the proton tracks and spatial coordinates of the atomic
 128 interactions based on the *PHITS-KURBUC mode*. Note that the δ -rays coming into REG2 from
 129 REG1 and REG3 were considered to establish the secondary electron equilibrium.
 130



131
 132 **Figure 1. Simulation geometry and proton track structure in PHITS:** (A) is the geometry for
 133 estimating DNA damage yields, and (B) is the generated 10 proton tracks at 100, 10, and 1 MeV. The
 134 track-structure modes are turned on only in REG2. The cut-off energies for electrons and protons are
 135 set to 1.0 eV and 1.0 keV, respectively. In Fig. 1B, proton tracks were depicted using the constant
 136 thickness of REG2 (= 100 nm) as examples. When estimating the yields of DNA damage, the
 137 thickness of REG2 was defined to be large enough that at least 1% of the proton energy is being
 138 deposited in this region. Note that for proton energies larger than 1 MeV, a constant thickness of 1
 139 μm was chosen.

140
 141 Assuming that the number of the events (i.e., ionizations and excitations) per deposited
 142 energy $N_{\text{event}}/E_{\text{dep}}$ and that of linkage composed of two events within 10 bp (3.4 nm) per
 143 deposited energy $N_{\text{link}}/E_{\text{dep}}$ are proportional to the yields of strand breaks (SBs) and DSBs, the
 144 yields SBs and DSBs (Y_{SB} and Y_{DSB}) can be calculated as follows (36):

$$Y_{\text{SB}} = k_{\text{SB}} \frac{N_{\text{event}}}{E_{\text{dep}}}, \quad (1)$$

$$Y_{\text{DSB}} = k_{\text{DSB}} \frac{N_{\text{link}}}{E_{\text{dep}}}, \quad (2)$$

145 where k_{SB} and k_{DSB} are the coefficients for estimating the yields of SBs and DSB from the events
 146 and the linkages, respectively (keV/Gy/Da). These coefficients can be determined by fitting the
 147 experimental yields of SSB and DSB after exposure to photon beams (i.e., 220 kVp X-rays) as
 148 reported previously (32). Induction of indirect DNA damage by radical species, such as OH
 149 radicals, are implicitly considered in these coefficients, although the kinematics of the radicals
 150 are not explicitly reproduced in the model. The DBSCAN, which is similar as this model, is
 151 known as a simple approach which can obtain the SSB and DSB yields from events per cluster
 152 (30). Unlike the algorithms of DBSCAN, the present model focuses on only scoring the number
 153 of events and distance between two events (32). This model does not need to classify the cluster
 154 and noise from spatial distributions of atomic interactions, which is expected to reduce
 155 computational time. It should be noted that the implicit consideration of chemical reactions in
 156 this model has some drawbacks, i.e., the influence of LET is not accounted for explicitly.

157 Because of the update of *etsmode* for electron kinetic energy higher than 100 keV in the
 158 latest PHITS ver. 3.27, we redetermined these coefficients so as to reproduce the experimental
 159 yields of SSB and DSB after 220-kVp X-rays exposure (40,41) (here, $k_{\text{SB}} = 6.46 \times 10^{-12}$ keV
 160 $\text{Gy}^{-1}\text{Da}^{-1}$, $k_{\text{DSB}} = 1.48 \times 10^{-13}$ keV $\text{Gy}^{-1}\text{Da}^{-1}$). The benchmark test for the model performance
 161 was remade for monoenergetic electrons (Fig. S1) and for photon beams (Fig. S2A), where we
 162 confirmed that the yields of electron-induced SSB and DSB estimated using the updated
 163 parameters showed the same results as those reported previously (32). Note that the yield of
 164 SSBs, Y_{SSB} , can be obtained by subtracting $2 \times Y_{\text{DSB}}$ from Y_{SB} . Using this simplified DNA
 165 damage estimation model with the updated parameters, we calculated the Y_{SSB} and Y_{DSB} for
 166 various proton kinetic energies. The number of simulated particles was adapted to reach a
 167 statistical uncertainty of less than 1%. The estimated DSB yields were compared with other
 168 simulation results (i.e., Geant4-DNA, original KURBUC and PARTRAC) (30,42,43) and the
 169 corresponding experimental data (using cultured cells and plasmid DNA) (30,44-46) in the
 170 literature. The detail of the comparative data is summarized in Table S1.

171

172 2-3. Estimation of DSB complexity

173 Assuming that the number of events (i.e., ionizations and excitations) is proportional to
 174 the yield of SB, we also classified the DSB complexity from a simplified cluster analysis using
 175 the number of events within a 10-bp (3.4 nm) diameter at a DSB site (a gravity of linkage), N_{cl}
 176 (33). We deduced that 12 events were needed on average to induce an additional SB at a DSB
 177 site to reproduce the experimental complex DSB measured by atomic force microscopy (33).
 178 In the same manner as that for the model for estimating SSB and DSB yields, we updated the
 179 criteria for determining complex DSB, i.e., DSB+ (a DSB coupled with an SB) and DSB++ (a
 180 DSB coupled with two SBs). The number of ionization and excitations at a DSB site (i.e., a

181 sphere with a 3.4-nm radius) increased by about 1% because of the update of *etsmode* by the
 182 recent PHITS development. Therefore, when estimating the DSB complexity, we used the
 183 following criteria: simple DSB (sDSB) for $2 \leq N_{cl} \leq 14$, DSB+ for $14 < N_{cl} \leq 26$ and DSB++
 184 for $N_{cl} > 26$. The benchmark results for this update are summarized in Fig. S2B, where it is also
 185 confirmed that the updated parameters enabled the estimation of a similar tendency as reported
 186 previously (34). Using the same geometry illustrated in Fig. 1A and this simplified model, we
 187 estimated the contents of DSB+ and DSB++ for 10 keV electrons, 30 MeV protons, 2 MeV
 188 protons and 1 MeV protons and compared them with the simulation data calculated by the
 189 original KURBUC (42) and Geant4-DNA (47). In the same manner as that for the DSB yields,
 190 DSB complexity was calculated with sufficient numbers of particles to make the statistical
 191 uncertainty less than 1%.

192

193 2-4. RBE values for early SSB and DSB induction

194 The RBE values for SSB and DSB, referred to as RBE_{SSB} and RBE_{DSB} , respectively, were
 195 calculated using the *PHITS-KURBUC mode*. We selected 200 kVp X-rays (0.5-mm Al + 0.5-
 196 mm Cu filtration) as the reference radiation throughout this study. This kind of 200 kVp X-rays
 197 with such filtration is often used in the field of radiation biology. The DNA damage yields
 198 immediately after irradiation are proportional to the absorbed dose (48,49). Regarding this, the
 199 RBE_{SSB} and RBE_{DSB} were calculated using the following equations.

$$RBE_{SSB} = \frac{Y_{SSB}}{Y_{SSB(200\text{-kVp X-rays})}}, \quad (3)$$

$$RBE_{DSB} = \frac{Y_{DSB}}{Y_{DSB(200\text{-kVp X-rays})}}, \quad (4)$$

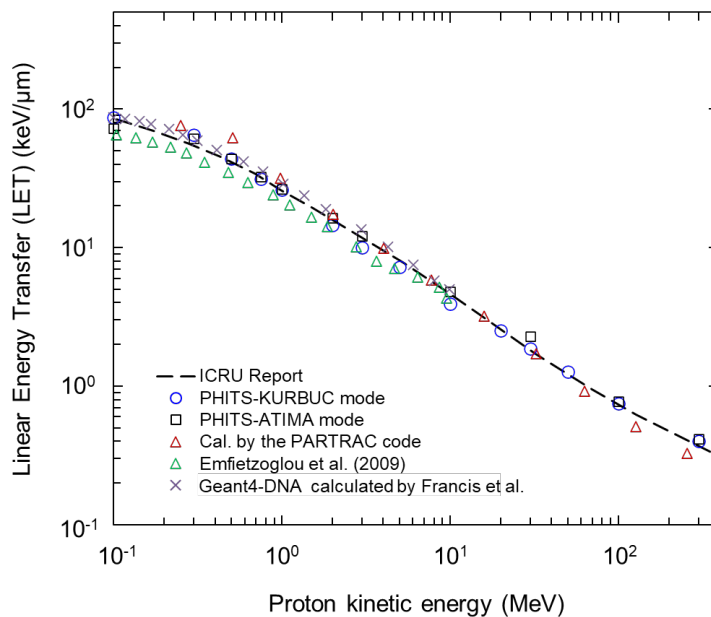
200 where Y_{SSB} and Y_{DSB} are the SSB and DSB yields for any radiation, respectively; $Y_{SSB(200\text{-kVp X-}}$
 201 $rays)$ and $Y_{DSB(200\text{-kVp X-rays})}$ are the SSB and DSB yields for the 200 kVp X-rays. The estimated
 202 yields of Y_{SSB} and Y_{DSB} as a function of LET were compared with the available experimental
 203 data (16,18,30,44-46,53-56,58) and the other simulation data (42,43,47,50-52). The data list
 204 used for this comparison is summarized in Table S1. It should be noted that the simulation data
 205 by the MCMS algorithm was calculated in this study (51,52). From the comparison, we
 206 evaluated the RBE values for DNA damage induced by proton beams.

207 The LET values are also calculated to investigate the relationship between LET and RBE
 208 for DSB (RBE_{DSB}). Figure 2 shows the relations between proton kinetic energy and stopping
 209 power (LET) for the *PHITS-KURBUC mode*, which were compared with the recommended
 210 data of the International Commission on Radiation Units and Measurements (ICRU) Report 49
 211 (60), other simulations (61-63), and the PHITS condensed-history mode of ATIMA. It should
 212 be noted that the LET for ATIMA mode was obtained by the t-LET tally, which can provide
 213 information on track length and dose as a function of the LET of a given material. As shown in
 214 Fig. 2, it was confirmed that the stopping power (LET) of the *PHITS-KURBUC mode* agrees

215 well with that of the condensed-history ATIMA mode and the ICRU Report 49 (60).

216 We also compared the RBE_{DSB} estimated by PHITS with the experimental RBE_{DSB} using
217 proton energy as a parameter to evaluate the accuracy of the PHITS simulation. We recalculated
218 the DSB yields by γ -rays (^{60}Co and ^{137}Cs sources), kVp X-rays (30-250 kVp), ultra-soft X-rays
219 (Ti_K , Al_K , Cu_L , and C_K), monoenergetic electrons and monoenergetic protons on the basis of
220 the current DNA damage model. For the simulation for monoenergetic electrons, we simulated
221 whole electron tracks using *etsmode*. When calculating the yields of photon beams, γ -rays and
222 kVp X-rays were incident to a water cuboid ($10 \times 10 \times 0.1 \text{ cm}^3$) surrounded by air as shown in
223 Fig. S3. The track-structure mode was activated in liquid water (REG2 in Fig. S3), while the
224 condensed-history approach was taken in air (REG1 in Fig. S3). For the monoenergetic protons,
225 the particles were incident to liquid water, as shown in Fig. 1. Note that the simulation setup is
226 the same as that for the simulation for monoenergetic protons used in Fig. 1. The PHITS results
227 were compared with the experimental data (16,18,30,44-46,53-56,58). The RBE_{DSB} was
228 calculated using 200 kVp X-rays as reference radiation.

229



230

231 **Figure 2. LET value as a function of proton kinetic energy.** The *PHITS-KURBUC mode* (open
232 blue circle) results are compared with the recommended data of ICRU Report 49 (60), other
233 simulations (61-63), and the PHITS condensed-history mode of ATIMA. Note that the LET for the
234 ATIMA mode is obtained by the t-LET tally.

235

236 2-5. Measurement of the cross-sections of cell nuclei

237 We measured the cross-section of cell nuclei of various cell lines in this study to grasp
238 the experimental condition using cultured cells. We used five types of cell lines: Chinese
239 Hamster fibroblast cell line V79-379A (IFO50082, JCRB Cell Bank, Japan), human lung
240 fibroblast cell line WI-38 (RCB0702, RIKEN, Japan), human lung bronchial epithelial cell line
241 HBE3-KT (CRL-4051, ATCC, Manassas, VA, USA), human prostate cancer (DU145), and non-
242 small cell lung cancer A549 (RCB3677, RIKEN Cell Bank, Japan). The V79-379A cells were

243 maintained routinely in Dulbecco's modified Eagle's medium (DMEM) (D0819, Sigma Life
244 Science) supplemented with 10% fetal bovine serum (FBS) and 1% penicillin/streptomycin
245 (p/s) (Sigma Life Science). The WI-38 cells and the A549 cells were maintained in the
246 DMEM/Nutrient Mixture F-12 (DMEM/F12) (D8437, Sigma Life Science) supplemented with
247 10% FBS (FBS, Equitech-Bio Inc.) and 1% p/s. The HBEC3-KT cells were maintained in a
248 bronchial epithelial cell medium (3211NZ, ScienCell). DU145 cells were grown in RPMI-1640
249 with L-glutamine (Thermo Fisher Scientific Inc.) supplemented with 10% FBS (FBS, Equitech-
250 Bio Inc.) and 1% p/s. All cells were maintained at 37°C in a humidified atmosphere of 95%
251 air/5% CO₂.

252 All cells were fixed in 4% paraformaldehyde for 10 min on ice and were then
253 permeabilized in 0.2% v/v Triton X-100 in phosphate-buffered saline (PBS) for 5 min. After
254 rinsing with PBS, the cells were incubated with 1 µg/ml DAPI solution (62248, Thermo Fisher
255 Scientific) for 15 min. After rinsing with PBS, the cells were observed using a high standard
256 all-in-one fluorescent microscope (BZ-9000; Keyence, Osaka, Japan). The sizes of the cell
257 nuclei were measured using the ImageJ software (64). The microscopic images of stained cell
258 nuclei and the histogram of the cross-sections are shown in Fig. S4A and Fig. S4B, respectively,
259 (see supplementary material), from which we calculated the mean radii of the ellipsoidal section
260 of the cell nuclei for all cell lines. Information on cell nucleus size was used for this DNA
261 damage simulation.

262

263 2-6. DNA damage simulation for PBT considering cell geometry

264 Using the mean radii measured by DAPI staining, we estimated the cell geometry, as
265 shown in Fig. S4A. The thickness of the cell cannot be measured by the microscopy used in
266 this study because of the spatial resolution of the z-stack. Thus, we used the ratio between the
267 mean radius of the ellipsoidal section of a cell nucleus and the thickness of the cell cytoplasm
268 shown in the literature (65). The geometry of the cytoplasm was assumed as half of an ellipse
269 with a constant 5-µm thickness. In this simulation, we used the cross-section of the lung
270 fibroblast cell lines, i.e., V79-379A and WI-38. We also measured the cross-sections for a few
271 additional cell lines (i.e., HBE3-KT, DU145 and A549). However, no relevant differences were
272 observed among these cell lines (Fig. S4B).

273 For the DNA damage simulation for PBT, we first reproduced the monoenergetic 60
274 MeV proton beam line reported by Chaudhary et al (58). In reproducing percentage of depth
275 dose (PDD) of the 60 MeV proton beams, we assumed a 0.8% standard deviation of the incident
276 proton energy when accelerated. The proton beams were incident to a water cube (40 × 40 × 40
277 cm³). We scored the energy spectra of proton beam at each depth to efficiently calculate the
278 yields, and the protons were simulated using the spectra and the cell geometry (see Fig. S5).
279 The thickness of the culture dish (C₈H₈)_n, 1.00 g/cm³) was set to 1 mm. The track-structure
280 modes (i.e., *etsmode* and *PHITS-KURBUC*) were activated within the cell, whereas the ATIMA
281 and EGS modes were used in the geometry except for the inside of the cell. The cut-off energies

282 of electrons were set to be 1 keV and 7 eV for the EGS mode and *etsmode*, respectively.
 283 Meanwhile, the proton cut-off energy was set to 1 keV. Using the simulation setup, we
 284 estimated the depth-dependence of the DSB yields, and compared the PHITS results with the
 285 experimental DSB yield measured by the 53BP1 focus formation assay in the literature (58).

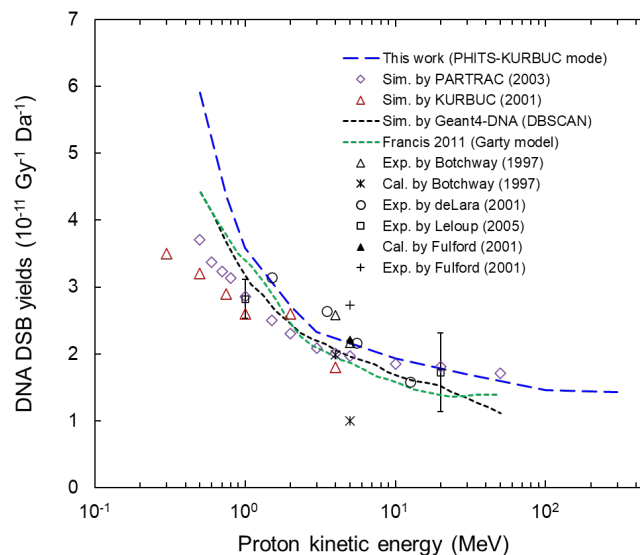
286

287 3. RESULTS AND DISCUSSION

288 3-1. Energy-dependence of DNA damage yields

289 Figure 3 shows the DSB yields estimated by the *PHITS-KURBUC mode*, which were
 290 compared with other available simulations (30,42,43) and the experimental data (30,44-46).
 291 The LET dependencies of the yields of SSB and DSB estimated by the PHITS code are also
 292 shown in Fig. S6. The PHITS estimation was performed using the geometry shown in Fig. 1.
 293 We also calculated the DSB yields using the cell geometry where the thickness of track-
 294 structure region is more than 1 μm to check the impact of the secondary electron equilibrium
 295 (see Fig. S7A). The DSB yields for high-energy protons (e.g., 100 MeV protons) are expected
 296 to be reduced when the equilibrium is violated; however, we observed no significant reduction.
 297 From these preliminary results, the DNA damage yields can be estimated under the charged
 298 particle equilibrium using the simulation setup shown in Fig. 1. In Fig. 3, the experimental data
 299 used for this comparison are composed of *in vitro* experiments with fibroblast cell lines (such
 300 as V79 cell line) and with plasmid DNA. The estimation of the KURBUC and the PARTRAC
 301 codes consider the indirect DNA damage induction by chemical processes such as that of the
 302 hydroxyl radical (OH radical).

303



304

305 **Figure 3. DSB yield in dependence on proton kinetic energy.** The results of this work (blue dotted
 306 line) are estimated using the *PHITS-KURBUC mode* and the DNA damage estimation model. The
 307 PHITS estimation is compared with the available simulation data (30,42,43) and the experimental
 308 data (30,44-46). Note that the experimental data are composed of V79 cells (Botchway et al, 1997;
 309 deLara et al, 2001) and plasmid DNA (Fulford et al, 2001; Leloup et al, 2005). The experimental data
 310 by deLara are taken from Francis et al (2011) (30).

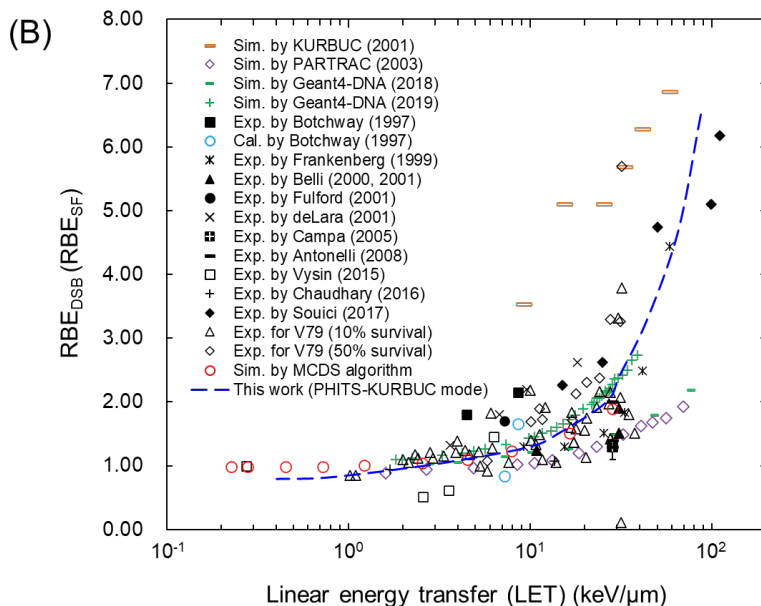
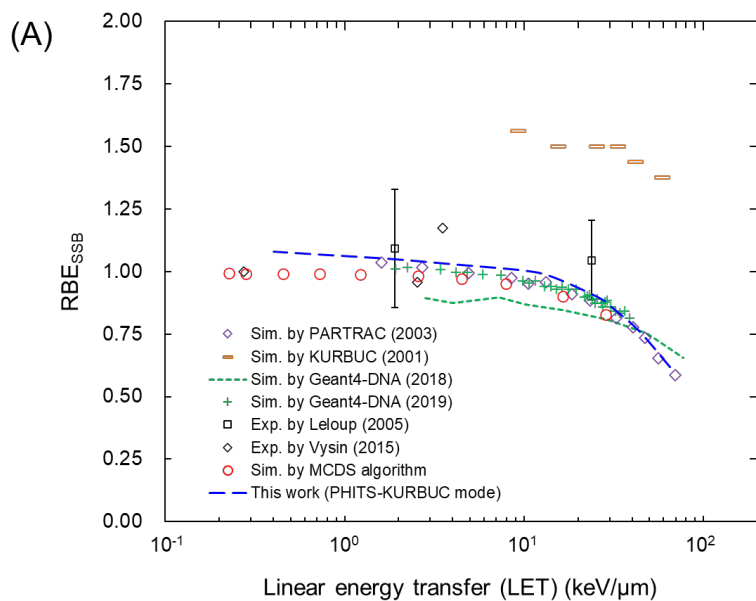
311
312
313
314
315
316
317
318
319
320
321
322
323
324
325
326
327
328
329
330
331
332
333
334
335
336
337
338
339
340
341
342
343
344
345
346
347
348
349

As shown in Figs. 3 and S5, the DSB yield increased as the proton kinetic energy decreased, and the PHITS estimation reasonably reproduced the experimental results ($R^2 = 0.593$). Meanwhile, focusing on protons with energies lower than 1 MeV, the DSB yields estimated by the PHITS code were higher than the published simulation results. However, there are no experimental results for monoenergetic protons with energies lower than 1 MeV. Thus, biomaterials have to be very thin, and the plasmid DNA under dry conditions must be suitable to obtain the experimental yields for such low-energy protons. Considering these, for the energy regime where experimental value measured in liquid water are available, the DNA damage estimation based on the simplified model is sufficient for reproducing the experimental DSBs.

On the other hand, the DSB yields for low-energy protons calculated by *PHITS-KURBUC mode* are higher than the corresponding data obtained from the other simulations considering chemical processes (KURBUC and PARTRAC) (42,43). This discrepancy is probably attributable to the fact that the coefficients for estimating the yields of SBs and DSB (k_{SB} and k_{DSB}) were determined to reproduce those of electron-induced DNA damage, i.e., our model intrinsically assumes that the ratios between radical recombination and indirect DNA damage induction are independent of the radiation type. This assumption may result in the inaccuracy in the DNA damage estimation for high LET radiation because the yields of OH radicals within a certain volume, which are related to the probabilities of radical recombination, increase with increasing LET. Therefore, further development of the model considering this LET dependence is desirable in future studies (66). However, because no experimental data are available for the DSB yields of protons with energies lower than 1 MeV, the accumulation of experimental data is also essential in the future.

3-2. LET dependence of RBE value for protons

We compared the RBE for SSB and DSB with the data available in the literature to further evaluate the yields of DNA damage estimated by the PHITS code. The PHITS simulation was performed using the geometry shown in Fig. 1. Figure 4A and 4B show the LET dependence of the RBE values estimated by the *PHITS-KURBUC mode* for SSB and DSB, respectively, where the PHITS estimation was compared with available experimental data (16,18,30,44-46,53-56,58) and other simulation data (42,43,47,50-52). Note that the reference radiation of the PHITS estimation was the 200-kVp X-rays with 0.5-mm Al and 0.5-mm Cu filtration (which is often used in cell experiments), whereas those for the data in the literature varied. The biological effects also depended on photon energy (59). Only a limited amount of the experimental RBE values, which are measured using specific photon energy (i.e., ^{60}Co γ -rays or 200 kVp X-rays), are available. For a precise comparison of the PHITS results and the experimental data, accumulating experimental data on DNA damage yields in the near future is necessary.



350

351

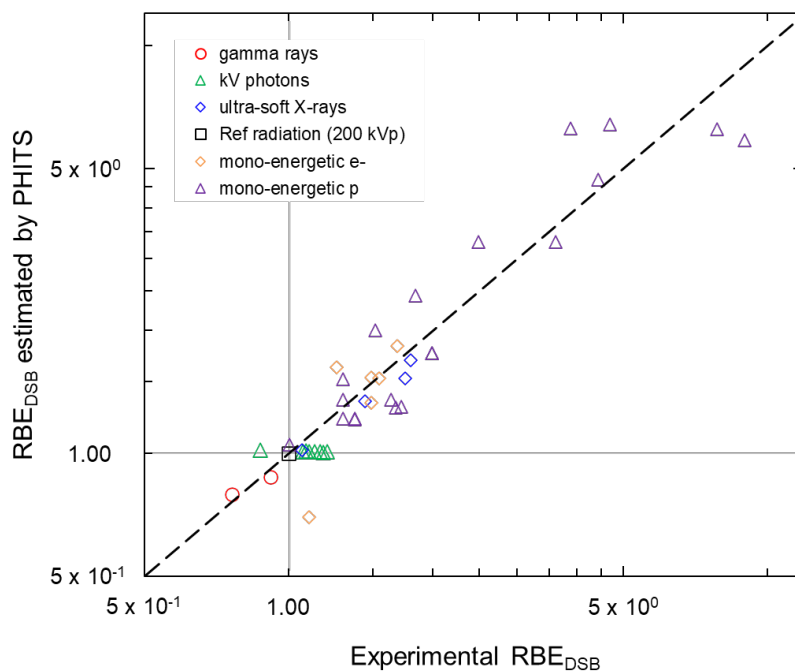
352 **Figure 4. LET dependence on RBE values.** (A) is the RBE for SSB and (B) is the RBE for DSB.
 353 The reference radiation of the PHITS estimation is the 200-kVp X-rays with 0.5-mm Al and 0.5-mm
 354 Cu filtration. The estimations by the PHITS code are compared with the available experimental data
 355 (16,18,30,44-46,53-56,58) and other simulation data (42,43,47,50-52).

356

357 In Fig. 4, RBE_{SSB} gradually decreased as the LET increased, whereas RBE_{DSB} gradually
 358 increased as the LET increases. Considering the large uncertainties of RBE values in the
 359 literature, the PHITS estimation reasonably agreed with the experimental and the other
 360 simulated data. Focusing on the high-LET region (i.e., greater than approximately 30 keV/μm),
 361 the RBE_{DSB} rapidly increased. The experimental RBE_{DSB} for the comparison in the high-LET
 362 region (closed diamonds ranging from 30 to 110 keV/μm in Fig. 4) were measured by plasmid
 363 DNA under dry conditions (16). As shown in Fig. 4, the PHITS simulation showed a similar
 364 tendency as that of the experimental RBE_{DSB} even in the high-LET region. For high-LET
 365 radiation, the DSB yields may be reduced by the release of fragments (67) (as well as multiple

366 DSBs (68)). In future development, it is needed to consider fragment release in this model.

367 Figure 5 shows the relationship between the RBE_{DSB} estimated by the PHITS code and
368 the corresponding experimental values. In drawing this graph, the DSB yields for γ -rays (^{60}Co
369 and ^{137}Cs sources), kVp X-rays (30–250 kVp), ultra-soft X-rays (Ti_K , Al_K , Cu_L , and C_K),
370 monoenergetic electrons and monoenergetic protons were recalculated. Note that the
371 experimental RBE_{DSB} values for electrons and photons were obtained from our previous paper
372 (32). Thus, a reasonable recreation of the experimental behaviour was found ($R^2 = 0.748$). Note
373 again that the experimental values for the high-LET protons were measured using dry DNA.
374



375 **Figure 5. Comparison of the experimental RBE for DSB and the PHITS estimation.** The
376 reference radiation of the PHITS estimation is the 200-kVp X-rays with 0.5-mm Al and 0.5-mm Cu
377 filtration. The RBE values calculated by PHITS are compared with the corresponding experimental
378 values (16,18,30,44-46,53-56,58).
379

380 3-3. Depth dependence of RBE for PBT

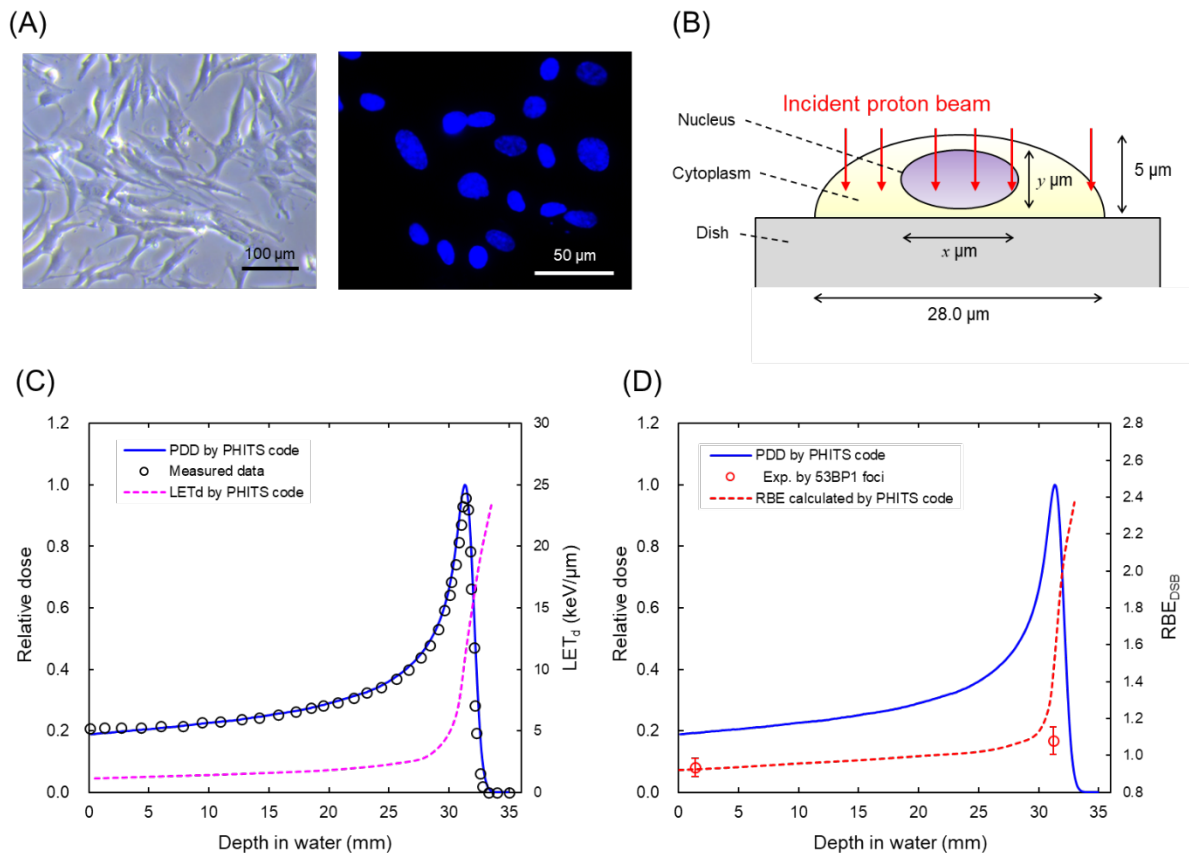
381 According to the comparison of the DSB estimation by the PHITS and various available
382 data in the literature, we then estimated the RBE_{DSB} value as a function of depth for the 60 MeV
383 PBT. In this simulation, we considered the cell geometry. Figure 6A and 6B shows the examples
384 of microscopic images of the fibroblast cells of WI-38 (shape and the stained nucleus) and the
385 simple geometry, respectively.
386

387 Figure 6C shows the PDD of the 60 MeV protons, where the blue solid line and open
388 circle are the simulated and measured PDD (58), respectively. The dose-averaged LET (noted
389 as LET_d) is also depicted as a function of the depth. The red dashed line in Fig. 6D shows the
390 depth dependence of RBE_{DSB} estimated by the *PHITS-KURBUC* mode using the cell geometry
391 shown in Fig. S5A, which was compared with the experimental data of 53BP1 foci (58). The
392 DSB yields were measured only at two positions: at a 1.38-mm depth for the entrance and a

393 31.5-mm depth for the Bragg peak. Focusing on the Bragg peak region, there is a subtle
394 discrepancy between the PHITS simulation and the experimental data. Considering that the
395 experimental uncertainties are shown as the standard error of the mean (s.e.m.), the inherent
396 uncertainties of nuclear foci (standard deviation) are expected to be much higher than the s.e.m.
397 Note that the standard deviations of the simulation results are less than 1%. In addition, the
398 number of foci per nucleus dramatically changes at the Bragg peak region. Considering this,
399 the uncertainty of placing a cell culture dish must be involved in the subtle difference.
400 Meanwhile, the protein of 53BP1 at the DSB site involves binding to the phosphorylated histone
401 H2AX (69) and regulating the repair balance between nonhomologous end joining and
402 homologous recombination (70). The efficiency of detecting complex DSB yields by such
403 biomarkers remains uncertain. Considering these, the overestimation by the simple model in
404 the PHITS code is reasonable. Recently, a different model based on ion cluster size in the
405 TOPAS-nBio (31) was proposed for directly using DNA damage estimation in the field of
406 medical physics. To obtain better agreement with the experimental results, the methodology of
407 the TOPAS-nBio will be useful for the future model development of the PHITS code.

408 As a preliminary study, the impact of the experimental geometry on DSB yield was also
409 investigated by comparing to the benchmark results shown in Fig. 3. Using the cell geometry
410 obtained from the DAPI staining of the cell nuclei, we estimated the LET dependence of the
411 DSB yields. Figure S7A shows that the DSB yields calculated using the cell geometry (Fig.
412 S5A) show a tendency similar to that in Fig. 3, which was calculated using the simple geometry
413 in Fig. 1. From Fig. S7A, the yields considering the cell geometry for 750 keV protons are
414 approximately 11% higher than those shown in Fig. 3 (benchmark data). This is due to the
415 attenuation of proton energy when passing through cells. Meanwhile, we also considered a
416 representative experimental geometry using plasmid DNA, where the plasmid DNA on the
417 glass slide was surrounded by voids (Fig. S5B). As shown in Fig. S7B, the DSB yields for the
418 plasmid DNA experiment are lower than those for the cell geometry in the low-LET region.
419 This is because the secondary electron equilibrium does not hold for the plasmid DNA
420 experiment. From these preliminary simulation results, we also confirmed that the PHITS code
421 enables predicting DSB yields for various experimental conditions such as cultured cells and
422 plasmid DNA in voids.

423
424



425

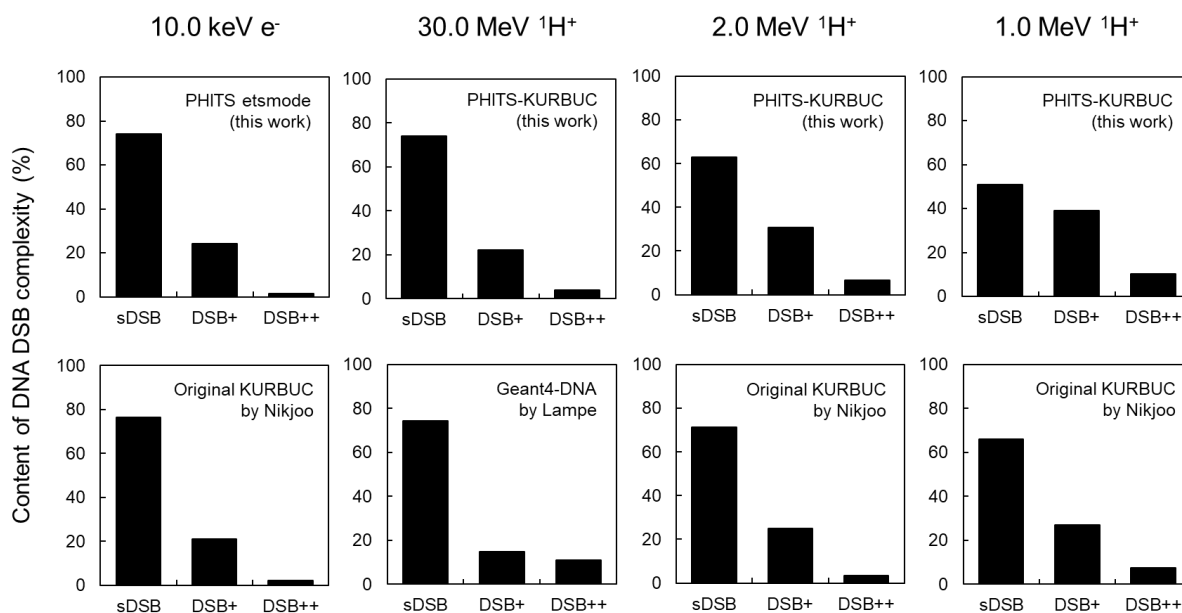
426 **Figure 6. DSB estimation for the 60 MeV PBT.** (A) shows an example of microscopic images and
 427 the cell nucleus of WI-38 stained by DAPI. (B) is the cell geometry considered in the PHITS code.
 428 (C) The PDD and LET of the 60 MeV PBT. (D) shows the depth dependence of RBE_{DSB} estimated
 429 by the *PHITS-KURBUC mode*. In Fig. 6B, we use the nucleus sizes for V79-379A ($x = 11.0$ μm , $y =$
 430 3.89 μm) and WI-38 ($x = 11.8$ μm , $y = 4.16$ μm).

431

432 3-4. DSB complexity for electrons and protons

433 We finally estimated the yields of complex DSBs for 10 keV electrons, 30 MeV protons,
 434 2.0 MeV protons, and 1.0 MeV protons. Figure 7 shows the content rates of sDSB, DSB+, and
 435 DSB++ estimated by the *PHITS-KURBUC mode*, which were compared with the other
 436 simulation results by KURBUC (42) and Geant4-DNA (47). There are differences between the
 437 individual Monte Carlo approaches in terms of relative or absolute differences. Considering
 438 this, we calculated the percentages of complex DSBs (DSB+ and DSB++) for comparison. As
 439 shown in Fig. 7, the contents of complex DSBs by the PHITS code show the tendencies similar
 440 to those of the other simulations in the case of low-LET radiation (10 keV e^- , 30 MeV $^1\text{H}^+$, and
 441 2 MeV $^1\text{H}^+$). This may be because secondary electrons are major contributors to energy
 442 deposition. Meanwhile, focusing on the high-LET protons (1 MeV $^1\text{H}^+$), the PHITS code
 443 slightly overestimated the contents of complex DSBs in the same manner as that of the DSB
 444 yields (Fig. 3). The difference of the percentage between the PHITS code and other simulations
 445 are shown in Fig. S8, in which the difference for 1 MeV protons is the largest among 10 keV
 446 electrons, 30 MeV protons, 2.0 MeV protons, and 1.0 MeV protons. There is a possibility that

447 the other codes underestimated the amount of complex DSBs. However, considering the
 448 experimental data on DNA fragments released by high-LET ions, we should interpret that this
 449 is because the DNA damage estimation in PHITS does not consider the change in indirect DNA
 450 damage yields in relation to LET. Considering these, the LET dependence of indirect damage
 451 induced by chemical processes plays an important role in precisely understanding complex
 452 DSB induction after high-LET irradiation. In this regard, further development of a chemical
 453 model is needed in the future to reproduce the change of indirect damage induction. However,
 454 the present simple model implemented in PHITS is sufficient for estimating the yields for
 455 various DSB types for electrons and protons, as shown in Fig S9, showing the yields of sDSB,
 456 DSB+, and DSB++ for the 10 MeV electrons, 300 MeV protons, 100 MeV protons, 30 MeV
 457 protons, 10 MeV protons, and 3 MeV protons.
 458



459
 460 **Figure 7. Estimation of DBS complexity (sDSB, DSB+, and DSB++).** The upper histograms are
 461 the contents estimated by the *PHITS-KURBUC mode* (this work). The lower histograms are those
 462 estimated by KURBUC (42) and Geant4-DNA (47). The results of this work are calculated using the
 463 simple cluster analysis reported in a previous report (34).
 464

465 4. CONCLUSION

466 In this study, we evaluated the yields of SSBs, DSBs, and complex DSBs for protons
 467 using the PHITS track-structure mode. The PHITS code was able to reproduce the experimental
 468 and simulated yields of various DNA lesion types for protons with low LET (less than about 30
 469 keV/ μ m). From these comparisons, the current simplified DNA damage model is sufficient for
 470 estimating DNA lesion yields induced after protons with energies higher than 1 MeV (around
 471 the Bragg peak energy). Meanwhile, we found that the RBE for DSB depends on the
 472 experimental (irradiation) conditions in the case of high-LET protons, suggesting that further
 473 modellings of chemical processes and fragment releases are needed in future studies. In addition,

474 no experimental data on DSB yields for protons with energies lower than 1 MeV were available.
475 The accumulation of such experimental yields for high-LET radiations (such as α particles (71))
476 is needed in the future.

477 A major aim of this work was to apply the DNA damage estimation model dedicated for
478 electrons to simulations for proton beams. Meanwhile, our ultimate goal is to develop an all-in-
479 one package for estimating radiobiological effects based on early DNA damage simulation and
480 biophysical models. The present data on DSB yields would be useful as input information for
481 biophysical models for predicting cell killing after irradiation, such as microdosimetric-kinetic
482 (MK) model (72) and modified models (e.g., stochastic MK model (73,74) and integrated MK
483 model (75,76)). This code for calculating DNA damage yields after the proton irradiation will
484 be implemented in the PHITS package in the future. Further model developments such as the
485 dependence of DNA damage induction on LET and new experimental data for high-LET
486 particles in liquid water are essential for developing of DNA damage estimation model which
487 can be directly used for medical field.

488

489 **CONFLICT OF INTEREST**

490 The authors declare that they have no conflict of interest.

491

492 **FUNDING**

493 This work was supported by the Japan Society for the Promotion of Science KAKENHI (Grant
494 no. 19K17215, 22H03744), and was financially supported by the JAEA Fund for Exploratory
495 Researches (Houga fund).

496

497 **SUPPLEMENTARY MATERIALS**

498 The following are available online:

- 499 ▪ Figure S1: Benchmark test 1: DNA strand break yields for electrons,
- 500 ▪ Figure S2: Benchmark test 2: DNA damage yields by photon irradiation and DBS
501 complexity for electrons,
- 502 ▪ Figure S3: Simulation geometry for photon beams,
- 503 ▪ Figure S4: Measuring the size of cell nucleus,
- 504 ▪ Figure S5: Simulation geometries for cell experiment and plasmid experiment,
- 505 ▪ Figure S6: Benchmark test 3: DNA strand break yields for protons,
- 506 ▪ Figure S7: Estimation of proton-induced DSB yields considering geometries for cell
507 experiment and plasmid DNA experiment,
- 508 ▪ Figure S8: Difference of complex DSB between PHITS and other simulations
- 509 ▪ Figure S9: Estimation of yields of various DSB types for electrons and protons,
- 510 ▪ Table S1: List of references for DNA damage yields by proton irradiations.

511

512 **AUTHOR CONTRIBUTIONS**

513 Y. Matsuya designed this study. A. Parisi and Y. Matsuya discussed the characteristics of proton
514 particles and how to compare the simulation and the experimental data in literature. Y. Matsuya,
515 T. Kai and Y. Yoshii developed the present model for estimating strand breaks yield. A. Parisi
516 performed the calculations with the MCDS code. Y. Matsuya wrote the manuscript. T. Sato
517 supervised this study. All authors reviewed the manuscript.

518

519 REFERENCES

- 520 ¹ Levin, W.P., Kooy, H., Loeffler, J.S., DeLaney, T.F. Proton beam therapy. *Br. J. Cancer* 93,
521 849–854 (2005).
- 522 ² Matsumoto, Y. Relative Biological Effectiveness and Fractionation of Proton-Beam Therapy.
523 In: Tsuboi, K., Sakae, T., Gerelchuluun, A. (eds). *Proton Beam Radiotherapy: Physics and*
524 *Biology*. 1st ed. Springer Nature Singapore Pte Ltd., 209–222 (2020).
- 525 ³ Date, H., Sutherland, K.L., Hayashi, T., Matsuzaki, Y., Kiyanagi, Y. Inelastic collision
526 processes of low-energy protons in liquid water. *Radiat. Phys. Chem.* 75 179–187 (2006).
- 527 ⁴ Ödén, J., DeLuca, P.M., Orton, C.G. The Use of a Constant RBE=1.1 for Proton
528 Radiotherapy Is No Longer Appropriate. *Med. Phys.* 45 (2), 502–505 (2018).
- 529 ⁵ Paganetti, H. Nuclear interactions in proton therapy: dose and relative biological effect
530 distributions originating from primary and secondary particles. *Phys. Med. Biol.* 47 (5), p.747
531 (2002).
- 532 ⁶ Surova, O., Zhivotovsky, B. Various modes of cell death induced by DNA damage.
533 *Oncogene* 32, 3789–3797 (2013).
- 534 ⁷ Olive PL. The role of DNA single- and double-strand breaks in cell killing by ionizing
535 radiation. *Radiat. Res.* 150 (Suppl.), S42–S51 (1998).
- 536 ⁸ Carante MP, Altier S, Bortolussi S, Postuma I, Protti N, Ballarini F. Modeling radiation-
537 induced cell death: role of different levels of DNA damage clustering. *Radiat. Environ.*
538 *Biophys.* 54, 305–316 (2015).
- 539 ⁹ Ballarini F, Altieri S, Bortolussi S, Carante M, Giroletti E, Protti N. The BIANCA
540 model/code of radiation-induced cell death: application to human cells exposed to different
541 radiation types. *Radiat. Environ. Biophys.* 53, 525–533 (2014).
- 542 ¹⁰ Matsuya, Y., Sato, T., Nakamura, R., Naijo, S., Date, H. A theoretical cell-killing model to
543 evaluate oxygen enhancement ratios at DNA damage and cell survival endpoints in radiation
544 therapy. *Phys. Med. Biol.* 65, 095006 (2020).
- 545 ¹¹ Paganetti, H. Significance and Implementation of RBE Variations in Proton Beam Therapy.
546 *Technol. Cancer Res. Treat.* 2(5), 413-426 (2003).
- 547 ¹² Mori, R., Matsuya, Y., Yoshii, Y., H. Date. Estimation of the radiation-induced DNA double-
548 strand breaks number by considering cell cycle and absorbed dose per cell nucleus. *J. Radiat.*
549 *Res.* 59(3), 253–260 (2018).
- 550 ¹³ D’Abrantes, S., Gratton, S., Reynolds, P., Kriechbaumer, V., McKenna, J., Barnard, S.,
551 Clarke, D.T., Botchway, S.W. Super-Resolution Nanoscopy Imaging Applied to DNA

- 552 Double-Strand Breaks. *Radiat. Res.* 189, 19–31 (2018).
- 553 ¹⁴ Ushigome, T., Shikazono, N., Fujii, K., Watanabe, R., Suzuki, M., Tsuruoka, C., Tauchi, H.,
554 Yokoya, A. Yield of Single- and Double-Strand Breaks and Nucleobase Lesions in Fully
555 Hydrated Plasmid DNA Films Irradiated with High-LET Charged Particles. *Radiat. Res.* 177,
556 614–627 (2012).
- 557 ¹⁵ Shiina, T., Watanabe, R., Shiraishi, I., Suzuki, M., Sugaya, Y., Fujii, K., Yokoya, A.
558 Induction of DNA damage, including abasic sites, in plasmid DNA by carbon ion and X-ray
559 irradiation. *Radiat. Environ. Biophys.* 52, 99–112 (2013).
- 560 ¹⁶ Souici, M., Khalil, T.T., Muller, D., Raffy, Q., Barillon, R., Belafrites, A., Champion, C.,
561 Fromm, M. Single- and Double-Strand Breaks of Dry DNA Exposed to Protons at Bragg-
562 Peak Energies. *J. Phys. Chem. B.* 121, 497–507 (2017).
- 563 ¹⁷ Tamborino, G., Perrot, Y., De Saint-Hubert, M., Struelens, L., Nonnekens, J., De Jong, M.,
564 Konijnenberg M.W., Villagrasa, C. Modeling Early Radiation DNA Damage Occurring
565 During ¹⁷⁷Lu-DOTATATE Radionuclide Therapy. *J. Nucl. Med.* 63(5), 761–769 (2022).
- 566 ¹⁸ Vysin, L., Brabcova, K.P., Stepan, V., Moretto-Capelle, P., Bugler, B., Legube, G., Cafarelli,
567 P., Casta, R., Champeaux, J.P., Sence, M., Vlk, M., Wagner, R., Stursa, J., Zach, V., Incerti,
568 S., Juha, L., Davi' dkova', M. Proton-induced direct and indirect damage of plasmid DNA.
569 *Radiat. Environ. Biophys.* 54, 343–352 (2015).
- 570 ¹⁹ Nikjoo, H., Goodhead, D.T., Charlton, D.E. and Paretzke, H.G. Energy deposition in small
571 cylindrical targets by monoenergetic electrons. *Int. J. Radiat. Biol.* 60, 739–756 (1991).
- 572 ²⁰ Paretzke, H. G. Radiation track structure theory. In *Kinetics of Nonhomogeneous Processes*
573 (G. R. Freeman, Ed.), pp. 89–170. Wiley, New York (1987).
- 574 ²¹ Incerti, S. Baldacchino, G., Bernal, M., Capra, R., Champion, C., Francis, Z., Guatelli, S.,
575 Guèye, P., Mantero, A., Mascialino, B., Moretto, P., Nieminen, P., Rosenfeld, A., Villagrasa,
576 C., and Zacharatou, C. The Geant4-DNA project. *Int. J. Mod. Simul. Scien. Comput.* 01 (02),
577 157–178 (2010).
- 578 ²² Nikjoo, H., Emfietzoglou, D., Liamsuwan, T., Taleei, R., Liljequist, D., and Uehara, S.
579 Radiation track, DNA damage and response– a review. *Rep. Prog. Phys.* 79, 116601 (2016).
- 580 ²³ Friedland, W., Dingfelder, M., Kunderát, P., and Jacob, P. Track structures, DNA targets and
581 radiation effects in the biophysical Monte Carlo simulation code PARTRAC. *Mutat. Res.*
582 711, 28 (2011).
- 583 ²⁴ Yoshii, Y., Sasaki, K., Matsuya, Y., and Date, H. Cluster analysis for the probability of DSB
584 site induced by electron tracks. *Nucl. Instr. Methods Phys. Res. B.* 350, 55–59 (2015).
- 585 ²⁵ Incerti, S., Kyriakou, I., Bordage, M.C., Guatelli, S., Ivanchenko, V., and Emfietzoglou, D.
586 Track structure simulations of proximity functions in liquid water using the Geant4-DNA
587 toolkit. *J. Appl. Phys.* 125, 104301 (2019).
- 588 ²⁶ Xie, W., Li, J., Li, C., Qiu, R., Yan, C., Zeng, Z. Comparison of direct DNA strand break
589 simulated with different DNA models. *Radiat. Protect. Dosim.* 156(3), 283-288 (2013).
- 590 ²⁷ Meylan, S., Incerti, S., Karamitros, M., Tang, N., Bueno, M., Clairand, I., Villagrasa, C.

- 591 Simulation of early DNA damage after the irradiation of a fibroblast cell nucleus using
592 Geant4-DNA. *Sci. Rep.* 7(1), 1–15 (2017).
- 593 ²⁸ Nakano, H., Kawahara, D., Tanabe, S., Utsunomiya, S., Takizawa, T., Sakai, M., Nakano,
594 T., Ohta, A., Kaidu, M., Ishikawa, H. Calculated relative biological effectiveness (RBE) for
595 initial DNA double-strand breaks (DSB) from flattening filter and flattening filter-free 6 MV
596 X-ray fields. *BJR Open.* 3(1), 20200072 (2021).
- 597 ²⁹ Saito, A., Kawahara, D., Nakano, H., Nagata, Y. DNA strand breaks based on Monte Carlo
598 simulation in and around the Lipiodol with flattening filter and flattening filter-free photon
599 beams. *Reports of Pract Oncol Radiother.* Ahead of print (2022), doi:
600 10.5603/RPOR.a2022.0067
- 601 ³⁰ Francis, Z., Villagrasa, C., Clairand, I. Simulation of DNA damage clustering after proton
602 irradiation using an adapted DBSCAN algorithm. *Comput. Methods Programs. Biomed.*
603 101(3), 265–270 (2011).
- 604 ³¹ Ramos-Méndez, J., Burigo, L. N., Schulte, R., Chuang, C., Faddegon, B. Fast calculation of
605 nanodosimetric quantities in treatment planning of proton and ion therapy. *Phys. Med. Biol.*,
606 63(23), 235015 (2018).
- 607 ³² Matsuya, Y., Kai, T., Yoshii, Y., Yachi, Y., Naijo, S., Date, H., Sato, T. Modeling of yield
608 estimation for DNA strand breaks based on Monte Carlo simulations of electron track
609 structure in liquid water. *J. Appl. Phys.* 126, 124701 (2019).
- 610 ³³ Matsuya, Y., Nakano, T., Kai, T., Shikazono, N., Akamatsu, K., Yoshii, Y., Sato, T. A
611 Simplified Cluster Analysis of Electron Track Structure for Estimating Complex DNA
612 Damage Yields. *Int. J. Mol. Sci.* 21, 1701 (2020).
- 613 ³⁴ Matsuya, Y., Kai, T., Sato, T., Ogawa, T., Hirata, Y., Yoshii, Y., Parisi, A., Liamsuwan, T.
614 Track-structure mode in Particle and Heavy Ion Transport code System (PHITS): application
615 to radiobiological research. *Int. J. Radiat. Biol.* 98 (2), 148-157 (2022).
- 616 ³⁵ Sato, T., Iwamoto, Y., Hashimoto, S., Ogawa, T., Furuta, T., Abe, S., Kai, T., Tsai, P-E.,
617 Matsuda, N., Iwase, H., Shigyo, N., Sihver, L., and Niita, K. Features of Particle and Heavy
618 Ion Transport code System (PHITS) version 3.02. *J. Nucl. Sci. Technol.* 55(5-6), 684–690
619 (2018).
- 620 ³⁶ Matsuya, Y., Kai, T., Sato, T., Liamsuwan, T., Sasaki, K., Nikjoo, H. Verification of
621 KURBUC-based Ion Track Structure Mode for Proton and Carbon Ions in the PHITS Code.
622 *Phys. Med. Biol.* 66, 06NT02 (2021).
- 623 ³⁷ Ogawa, T., Hirata, Y., Matsuya, Y., Kai, T. Development of proton track structure model
624 applicable to arbitrary materials. *Sci. Rep.* 11, 24401 (2021).
- 625 ³⁸ Geissel, H., Scheidenberger, C., Malzacher, P., Kundendorf, J., Weick, H., ATIMA,
626 Germany: GSI; <http://web-docs.gsi.de/~weick/atima/> (accessed on May 2022)
- 627 ³⁹ Hirayama, H., Namito, Y., Bielajew, A.F., Wilderman, S.J., Nelson, W.R. The EGS5 Code
628 System; Office of Scientific and Technical Information (OSTI): Oak Ridge, TN (2005).
- 629 ⁴⁰ Ljungman, M., Nyberg, S., Nygren, J., Eriksson, M., Ahnstrom, G. DNA-bound proteins

630 contribute much more than soluble intracellular compounds to the intrinsic protection against
631 radiation-induced DNA strand breaks in human cells. *Radiat. Res.* 127, 171–176 (1991).

632 ⁴¹ Lobrich, M., Cooper, P.K., Rydberg, B. Non-random distribution of DNA double-strand
633 breaks induced by particle irradiation. *Int. J. Radiat. Biol.* 70, 493–503 (1996).

634 ⁴² Nikjoo, H., O’Neill, P., Wilson, W.E., Goodhead, D.T. Computational approach for
635 determining the spectrum of DNA damage induced by ionizing radiation. *Radiat. Res.* 156,
636 577–583 (2001).

637 ⁴³ Friedland, W., Jacob, P., Bernhardt, Ph., Paretzke, H.G., Dingfelder, M. Simulation of DNA
638 damage after proton irradiation, *Radiat. Res.* 159, 401–410 (2003).

639 ⁴⁴ Botchway, S.W., Stevens, D.L., Hill, M.A., Jenner, T.J., O’Neill, P. Induction and rejoining
640 of DNA double-strand breaks in chinese hamster V79-4 cells irradiated with characteristic
641 aluminum K and copper L ultrasoft X rays. *Radiat. Res.* 8, 317–324 (1997).

642 ⁴⁵ Leloup, C., Garty, G., Assaf, G., Cristova, A., Breskin, A., Chechik, R., Shchemelinin, S.,
643 Paz-Elizur, T., Livneh, Z., Schulte, R.W., Bashkirov, V., Milligan, J.R., Grosswendt, B.
644 Evaluation of lesion clustering in irradiated plasmid DNA. *Int. J. Radiat. Biol.* 81(1), 41–54
645 (2005).

646 ⁴⁶ Fulford, J., Nikjoo, H., Goodhead, D.T., O’Neill, P. Yields of SSB and DSB induced in DNA
647 by AlK ultrasoft X-rays and α -particles: comparison of experimental and simulated yields.
648 *Int. J. Radiat. Biol.* 77(10), 1053–1066 (2001).

649 ⁴⁷ Lampe, N., Karamitros, M., Breton, V., Brown, J.M.C., Sakata, D., Sarramia, D., Incerti, S.
650 Mechanistic DNA Damage Simulations in Geant4-DNA Part 2: Electron and Proton Damage
651 in a Bacterial Cell. *Physica Medica* 48, 146–155 (2018).

652 ⁴⁸ Ljungman, M., Nyberg, S., Nygren, J., Eriksson, M., Ahnström, G. DNA-Bound Proteins
653 Contribute Much More Than Soluble Intracellular Compounds to the Intrinsic Protection
654 against Radiation-Induced DNA Strand Breaks in Human Cells. *Radiat. Res.* 127 (2), 171–
655 176 (1991).

656 ⁴⁹ Löbrich, M., Rydberg, B., Cooper, P.K. Repair of x-ray-induced DNA double-strand breaks
657 in specific Not I restriction fragments in human fibroblasts: joining of correct and incorrect
658 ends. *Proc. Natl. Acad. Sci. USA* 92, 12050–12054 (1995).

659 ⁵⁰ Henthorn, N.T., Warmenhoven, J.W., Sotiropoulos, M., Aitkenhead, A.H., Smith, E.A.K.,
660 Ingram, S.P., Kirkby, N.F., Chadwick, A.L., Burnet, N.G., Mackay, R.I., Kirkbyab, K.J.,
661 Merchant, M.J. Clinically relevant nanodosimetric simulation of DNA damage complexity
662 from photons and protons. *RSC Adv.* 9, 6845–6858 (2019).

663 ⁵¹ Semenenko, V.A., Stewart, R.D. Fast Monte Carlo simulation of DNA damage formed by
664 electrons and light ions. *Phys. Med. Biol.* 51 (7), 1693–1706 (2006).

665 ⁵² Stewart, R.D. Yu, V.K., Georgakilas, A.G., Koumenis, C., Park, J.H., Carlson, D.J. Effects
666 of Radiation Quality and Oxygen on Clustered DNA Lesions and Cell Death. *Radiat. Res.*
667 176 (5), 587–602 (2011).

668 ⁵³ Frankenberg, D., Brede, H.J., Schrewe, U.J., Steinmetz, C., Frankenberg-Schwager, M.,

- 669 Kasten, G., Pralle, E. Induction of DNA double strand breaks by 1H and 4He ions in primary
670 human skin fibroblasts in the LET range of 8 to 124 keV/mm. *Radiat. Res.* 151, 540–549
671 (1999).
- 672 ⁵⁴ Belli, M., Cherubini, R., Vecchia, M.D., Dini, V., Moschini, G., Signoretti, C., Simone, G.,
673 Tabocchini, M.A., Tiveron, P. DNA DSB induction and rejoining in V79 cells irradiated with
674 light ions: a constant field gel electrophoresis study. *Int. J. Radiat. Biol.* 76 (8) 1095–1104
675 (2000).
- 676 ⁵⁵ Belli, M., Cherubini, R., Vecchia, M.D., Dini, V., Esposito, G., Moschini, G., Sapora, O.,
677 Signoretti, C., Simone, G., Sorrentino, E., Tabocchini, M.A. DNA Fragmentation In
678 Mammalian Cells Exposed To Various Light Ions. *Adv. Space Res.* 27 (2) 393–399 (2001).
- 679 ⁵⁶ Campa, A., Ballarini, F., Belli, M., Cherubini, R., Dini, V., Esposito, G., Friedland, W.,
680 Gerardi, S., Molinelli, S., Ottolenghi, A., Paretzke, H., Simone, G., Tabocchini, M.A. DNA
681 DSB induced in human cells by charged particles and gamma rays: Experimental results and
682 theoretical approaches. *Int. J. Radiat. Biol.* 81(11), 841–854 (2005).
- 683 ⁵⁷ Antonelli, F., Belli, M., Cherubini, R., Dini, V., Esposito, G., Gerardi, S., Giardullo, P.,
684 Simone, G., Sorrentino, E., Tabocchini, M.A. DNA damage induced in human fibroblasts by
685 radiations of differing qualities. LNL annual report Appl. *Interdisciplinary Phys.* (2008).
686 https://www1.lnl.infn.it/~annrep/read_ar/2007/contributions/pdfs/051_B_32_B027.pdf
- 687 ⁵⁸ Chaudhary, P., Marshall, T.I., Currell, F.J., Kacperek, A., Schettino, G., K.M. Prise.
688 Variations in the Processing of DNA Double-Strand Breaks Along 60-MeV Therapeutic
689 Proton Beams. *Int. J. Radiat. Oncol. Biol. Phys.* 95(1) 86e94 (2016).
- 690 ⁵⁹ Okamoto, H., Kanai, T., Kase, Y. et al. Relation between lineal energy distribution and
691 relative biological effectiveness for photon beams according to the microdosimetric kinetic
692 model. *J. Radiat. Res.* 52, 75–81 (2011).
- 693 ⁶⁰ ICRU report 49. International Commission on Radiation Units and Measurements, Maryland,
694 USA: Bethesda (1993).
- 695 ⁶¹ Friedland, W., Schmitt, E., Kunderát, P., Dingfelder, M., Baiocco, G., Barbieri, S., Ottolenghi,
696 A. Comprehensive track-structure based evaluation of DNA damage by light ions from
697 radiotherapyrelevant energies down to stopping. *Sci. Rep.* 7, 45161 (2017).
- 698 ⁶² Emfietzoglou, D., Garcia-Molina, R., Kyriakou, I., Abri, I., Nikjoo, H. A dielectric response
699 study of the electronic stopping power of liquid water for energetic protons and a new I-value
700 for water. *Phys. Med. Biol.* 54, 3451–3472 (2009).
- 701 ⁶³ Francis, Z., Incerti, S., Karamitros, M., Tran, H.N., Villagrasa, C. Stopping power and ranges
702 of electrons, protons and alpha particles in liquid water using the Geant4-DNA package. *Nucl.*
703 *Instr. Methods Phys. Res. B* 269, 2307–2311 (2011).
- 704 ⁶⁴ Rasband, W. S., ImageJ, U. S. National Institutes of Health, Bethesda, Maryland, USA,
705 <http://imagej.nih.gov/ij/> (1997–2012).
- 706 ⁶⁵ Sakata, D., Suzuki, M., Hirayama, R., Abe, Y., Muramatsu, M., Sato, S., Belov, O., Kyriakou,
707 I., Emfietzoglou, D., Guatelli, S., Incerti, S., Inaniwa, T. Performance Evaluation for Repair

708 of HSGc-C5 Carcinoma Cell Using Geant4-DNA. *Cancers* 13, 6046 (2021).

709 ⁶⁶ Shin, W-G., Sakata, D., Lampe, N., Belov, P., Tran, N.H., Petrovic, I., Ristic-Fira, A.,
710 Dordevic, M., Bernal, M.A., Bordage, M-C., Francis, Z., Kyriakou, I., Perrot, Y., Sasaki, T.,
711 Villagrasa, C., Guatelli, S., Breton, V., Emfietzoglou, D., Incerti, S. A Geant4-DNA
712 Evaluation of Radiation-Induced DNA Damage on a Human Fibroblast. *Cancers*. 13, 4940
713 (2021).

714 ⁶⁷ Friedland, W., Jacob, P., Paretzke, H.G., Ottolenghi, A., Ballarini, F., Liotta, M. Simulation
715 of light ion induced DNA damage patterns. *Radiat. Prot. Dosim.* 122(1-4), 116–120 (2006).

716 ⁶⁸ Hunniford, C.A., McCullough, R.W., Davies, R.J.H., Timson, D.J. DNA damage by low-
717 energy ions. *Biochem. Soci. Trans.* 37(4), 893–896 (2009).

718 ⁶⁹ Ward, I.M., Minn, K., Jorda, K.G., Chen, J. Accumulation of Checkpoint Protein 53BP1 at
719 DNA Breaks Involves Its Binding to Phosphorylated Histone H2AX. *J. Biol. Chem.* 278 (22)
720 19579–19582 (2003).

721 ⁷⁰ Guo, X., Bai, Y., Zhao, M., Zhou, M., Shen, Q., Yun, C.H., Zhang, H., Zhu, W.G., Wang, J.
722 Acetylation of 53BP1 dictates the DNA double strand break repair pathway. *Nucleic Acids*
723 *Res.* 46(2), 689–703 (2018).

724 ⁷¹ Nikitaki, Z., Nikolov, V., Mavragani, I.V. Mladenov, E., Mangelis, A., Laskaratou, D.A.,
725 Fragkoulis, G.I., Hellweg, C.E., Martin, O.A., Emfietzoglou, D., Hatzi, V.I., Terzoudi, G.I.,
726 Iliakis, G., Georgakilas, A.G. Measurement of complex DNA damage induction and repair
727 in human cellular systems after exposure to ionizing radiations of varying linear energy
728 transfer (LET). *Free Radical Res.* 50 (Sup1), S64–S78 (2016).

729 ⁷² Hawkins, R.B. A statistical theory of cell killing by radiation of varying linear energy transfer.
730 *Radiat. Res.* 140, 366–374 (1994).

731 ⁷³ Sato, T., Furusawa, Y. Cell Survival Fraction Estimation Based on the Probability Densities
732 of Domain and Cell Nucleus Specific Energies Using Improved Microdosimetric Kinetic
733 Models. *Radiat. Res.* 178(4):341–356 (2012).

734 ⁷⁴ Sato, T., Hashimoto, H., Inaniwa, T., Takada, K., Kumada, H. Implementation of simplified
735 stochastic microdosimetric kinetic models into PHITS for application to radiation treatment
736 planning. *Int. J. Radiat. Res.* 97(10), 1450–1460 (2021).

737 ⁷⁵ Matsuya, Y., Sasaki, K., Yoshii, Y., Okuyama, G., Date, H. Integrated Modelling of Cell
738 Responses after Irradiation for DNA-Targeted Effects and Non-Targeted Effects. *Sci. Rep.*
739 8, 4849 (2018)

740 ⁷⁶ Matsuya, Y., McMahon, S.J., Ghita, M., Yoshii, Y., Sato, T., Date, H., Prise, K.M. Intensity
741 Modulated Radiation Fields Induce Protective Effects and Reduce Importance of Dose-Rate
742 Effects. *Sci. Rep.* 9, 9483 (2019).

743

744